PREPARATION OF COBALT NANOSTRUCTURES USING PULSED Nd: YAG LASER

PREPARACIÓN DE NANOESTRUCTURAS DE COBALTO UTILIZANDO UN LÁSER Nd:YAG PULSADO

Warkaa Omar Abed Al-Rashidy[1], Khalaf Ajaj[2*], Mushtaq Abed Al-Jubbori[3]

[1] Department of Pharmaceutical Chemistry, College of Pharmacy, Ninevah University, Mosul, Iraq.
[2] Ministry of Education, General Directorate of Education Ninevah, Mosul, Iraq.
[3] Department of Physics, College of Education for Pure Sciences, University of Mosul, 41001, Mosul, Iraq.

(Recibed: Feb./2025. Accepted: Sep./2025)

Abstract

This study presents the preparation and characterization of cobalt nanoscale particles, focusing on several of their physical properties. Cobalt nanostructures were synthesized using the Pulsed Laser Ablation in Liquid (PLAL) method, employing a Q-switched Nd: laser with a fundamental wavelength of 1064 nm, a pulse duration of 10 ns, and a repetition rate of 1 Hz. Laser ablation energies of 200 and 400 mJ, along with varying pulse counts of 100, 200, and 300 per energy setting, were used for synthesis. The measured physical properties include optical absorbance, absorption coefficient, energy gap, refractive index, and extinction coefficient. Three energy gap values, 1.53, 2.36, and 3.53 eV, were observed, showing a slight increase with the total number of pulses, with minimal influence from the pulse energy. Other optical parameters, including refractive index, absorption coefficient, extinction coefficient, and optical conductivity, exhibited an increasing trend with a higher total number of pulses.

Keywords: cobalt nanoparticles, laser ablation, physical properties of nanostructures.

* khalaf.aj.hussein@st.tu.edu.iq doi: https://doi.org./10.15446/mo.n72.118854

Resumen

Este estudio presenta la preparación y caracterización de nanopartículas de cobalto, centrándose en varias de sus propiedades físicas. Las nanoestructuras de cobalto se sintetizaron mediante la técnica de ablación láser pulsada en líquido (PLAL, por sus siglas en inglés), empleando un láser Nd:YAG conmutado en Q, con una longitud de onda fundamental de 1064 nm, una duración de pulso de 10 ns y una frecuencia de repetición de 1 Hz. Se emplearon energías de ablación láser de 200 y 400 mJ, junto con diferentes números de pulsos (100, 200 y 300) para cada valor de energía. Las propiedades físicas medidas incluyen la absorbancia óptica, el coeficiente de absorción, la banda prohibida, el índice de refracción y el coeficiente de extinción. Se observaron tres valores de energía de banda (1,53; 2,36 y 3,53 eV), los cuales mostraron un ligero incremento con el número total de pulsos y una influencia mínima de la energía de ablación. Otros parámetros ópticos, como el índice de refracción, el coeficiente de absorción, el coeficiente de extinción y la conductividad óptica, mostraron una tendencia creciente al aumentar el número total de pulsos.

Palabras clave: nanopartículas de cobalto, ablación láser, propiedades físicas de las nanoestructuras.

Introduction

Nanoparticles are becoming increasingly important in everyday life. Their uses extend into many fields of life, which include medical [1–5], electronics [6–10], solar cells [11–15], water and air purification [16–20], batteries [21–25], cosmetics [26–30], pesticides [31–35], and many other applications. The most important nanoparticles from an application point of view include those of gold, silver, and iron oxides (Fe_2O_3 and Fe_3O_4), which are widely used for medical and biological purposes; titanium dioxide (TiO_2) and zinc oxide (ZnO) nanoparticles, which are used in sunscreens,

photocatalysis, and as pigments in paints; silicon (Si) nanoparticles, which are critical in electronics and photovoltaic cells; and carbon (C) nanoparticles, such as graphene and carbon nanotubes, which are used in a variety of applications, from electronics to composites.

Cobalt (Co) nanostructures are of significant importance due to their potential applications in new technologies and innovations. Cobalt nanostructures are used in lithium-ion batteries as cathode components, enhancing battery performance by providing high energy density and long cycle life. They are also being explored in supercapacitors and fuel cells for their electrochemical properties, where they improve charge–discharge rates and overall energy capacity [36, 37]. Due to their magnetic properties, cobalt nanoparticles are studied for medical applications, including magnetic resonance imaging (MRI) contrast enhancement. They also show potential in targeted drug-delivery systems, where they can be guided by magnetic fields to specific sites in the body [38, 39].

In renewable-energy applications, cobalt-based nanostructures are utilized as catalysts in water-splitting reactions to produce hydrogen fuel. Cobalt nanostructures support photocatalytic processes as well, where they help enhance the rate of reactions under light exposure, contributing to solar fuel production [40, 41].

Cobalt nanostructures can be produced by several methods. These include: chemical vapor deposition, solution-based chemical reduction, electrodeposition, thermal decomposition, hydrothermal synthesis, polyol process, template-assisted synthesis, and pulsed laser ablation in liquid (PLAL). Each method has its own merits and disadvantages. Furthermore, these methods are continually being developed to achieve greater simplicity, cost-effectiveness, availability, and final product quality [42–46].

With these aims in mind, this work attempts to report results of the preparation conditions and some physical properties of cobalt nanostructures produced using the PLAL method.

Experimental Setup and Measurements

Materials and methods

Cobalt nanostructures in this work are produced using the pulsed laser ablation in liquid (PLAL) method. This method is characterized for being a versatile and environmentally friendly method for producing nanoparticles, including metals, semiconductors, and oxides. The experimental setup is shown in Figure 1.

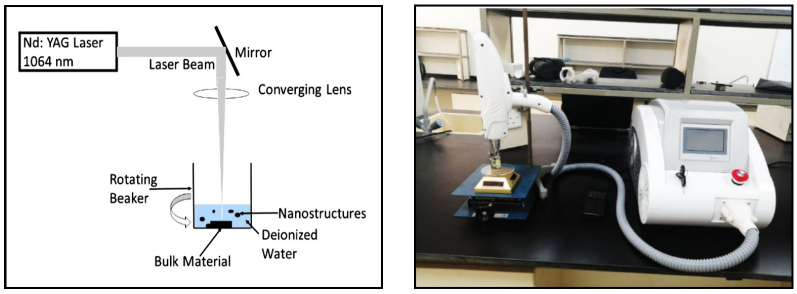

(a) *(b)*

FIGURE 1. *Experimental setup. (a) schematic diagram. (b) actual setup*

The laser used is a Q-switched Nd:YAG laser which can operate at pulsed wavelengths of 532, 1064, and 1320 nm. The per pulse energy can range between 20 and 2000 mJ, with a pulse duration of 10 ns. The pulse repetition rate can be varied between 1 and 10 Hz. The cobalt target rests at the bottom of the rotating water-containing beaker. The 1064 nm wavelength laser pulses directed and focused to 2 mm diameter on the cobalt target rapidly heat the target surface, causing material to vaporize and form a plasma plume, which condenses upon cooling, resulting in the formation of nanoparticles which then disperse into the surrounding liquid. Two energies of the laser pulses are used. These are 200 and 400 mJ/pulse, which correspond to 6.36 and 12.73 J/cm^2, respectively. Three values for the total number of pulses were applied. These were 100, 200, and 300 pulses. All runs were performed with the beaker containing the water and the target in rotation.

Measurements, Calculations and Results

Optical and UV-Vis absorption spectroscopy

Nano structures are extracted from the colloidal solution as droplets on well-cleaned and dried glass substrates, which were then dried at 85 °C, where the water is evaporated leaving the nanostructure. Optical and UV absorption spectroscopy are carried out using a UV-Visible 1800- doublebeam spectrophotometer, manufactured by Shimadzu, Japan. Measurements are performed at a speed of 400 nm/min. Optical properties measured include the absorbance (A), which is defined as the ratio of the absorbed optical beam intensity to the incident beam intensity.

$$A = \log_{10}\left(\frac{I_0}{I_T}\right) \tag{1}$$

The absorption coefficient (α) is defined through Lambert's law, given by

$$I_T = I_0 e^{-\alpha t} \tag{2}$$

where t is the sample thickness, and I_T is the transmitted beam intensity. The absorption coefficient α is related to the absorbance through the relation

$$\alpha = \frac{2.303A}{t} \tag{3}$$

Figure 2 shows the measured absorbance for the two pulse energies, with different numbers of pulses. The absorbance increases significantly with higher pulse numbers at 200 and 400 mJ, indicating an increased concentration or density of nanoparticles in the solution.

Corresponding results for the absorption coefficient calculated using equation(3) are presented in Figure3.

Both the absorbance and the absorption coefficient increase with increasing pulse energy and number of pulses.

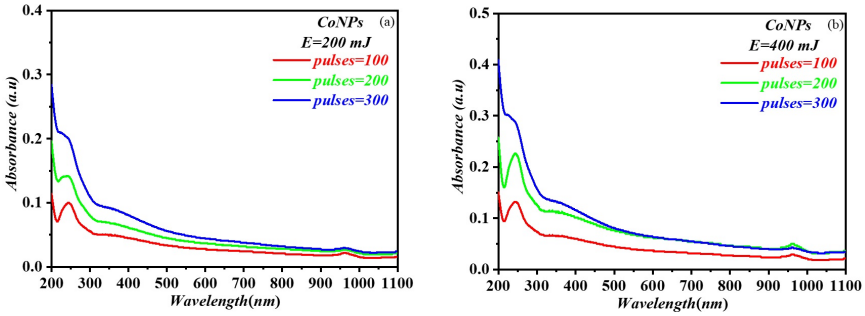

FIGURE 2. *The absorbance (a) for pulse energy 200 mJ and (b) 400 mJ*

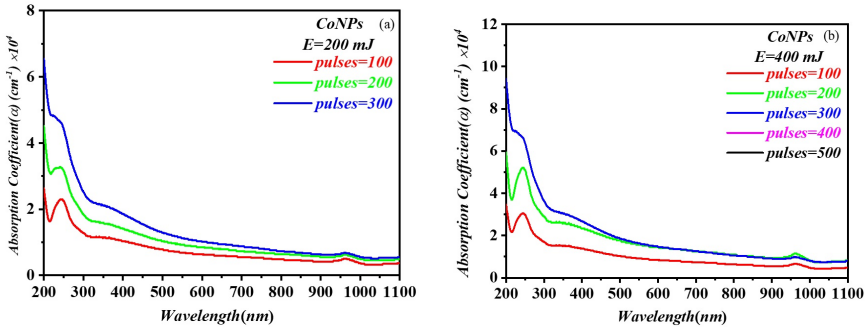

FIGURE 3. *The absorption coefficient (a) for pulse energy 200 mJ and (b) 400 mJ*

Measurement of the absorption coefficient opens the way for evaluation of the optical energy gap (E_g^{opt}), using Tauc's relation [47].

$$(\alpha.h\nu)^{\frac{1}{n}} = B\left[h\nu - E_g^{\text{opt}}\right] \tag{4}$$

B is a proportionality constant, which depends on the material. $(h\nu)$ is the photon energy in eV units. n is an exponent, which depends on the transition type. It takes the values of (1/2) and (3/2) for direct transitions and (2) and (3) for indirect transitions [48].

Figure 4 shows the evaluation of the optical energy gap values for samples prepared using laser pulse energies of 200, and 400 mJ, with three numbers of pulses of 100, 200, and 300 in each case. Three straight segments along the Tauc's relation plots using $n = 1/2$,

which corresponds to direct allowed transitions [49], were identified in each case. The energy gap is obtained from the intersection of the extrapolations with the x-axis. It is worth noting that all attempts to use other values for the exponent did not produce physically acceptable values for the energy gap. Relations of the energy gaps derived against the number of pulses at the two pulse energies are shown in Figure (5a, 5b). Comparison between both subfigures (a, b) shows no significant effect of the pulse energy on energy gaps values. However, both subfigures show systematic slight increases of each of the three energy gaps sets with increasing number of pulses. Published optical energy gap values for cobalt oxide nanostructures can vary based on synthesis methods and other experimental or data processing details. Nevertheless, evaluations using Tauc's extrapolation method suggest three distinct ranges for these energy gaps. The first set of values falls between 1.29 and 1.66 eV [50–52], with a mean and standard deviation of 1.5 eV. The second range spans 2.2 to 2.9 eV [53–55], with a mean and standard deviation of 2.4 eV. A third range, reported in reference [56], is between 3.53 and 3.65 eV, with a mean and standard deviation of 3.52 eV. Additionally, an outlying value of 4.07 eV is reported in reference [49]. The observed increase in energy gap values with increasing pulse count can be attributed to the reduction in particle size due to extended laser exposure. As the number of pulses increases, the nanoparticles undergo further fragmentation and surface refinement, leading to smaller crystallite sizes. This size reduction can induce quantum confinement effects, where the electronic band structure becomes size-dependent, resulting in wider bandgaps. This effect is particularly evident in the nanometer scale.

Other optical properties measured include the extinction coefficient (K), the refractive index (n), and the optical conductivity (σ). The extinction coefficient (K) of a particular optical wave length (λ) is defined as [57].

$$K = \frac{\alpha\lambda}{4\pi} \tag{5}$$

Figure 6 shows the calculated extinction coefficient plotted against wavelength for all experimental conditions.

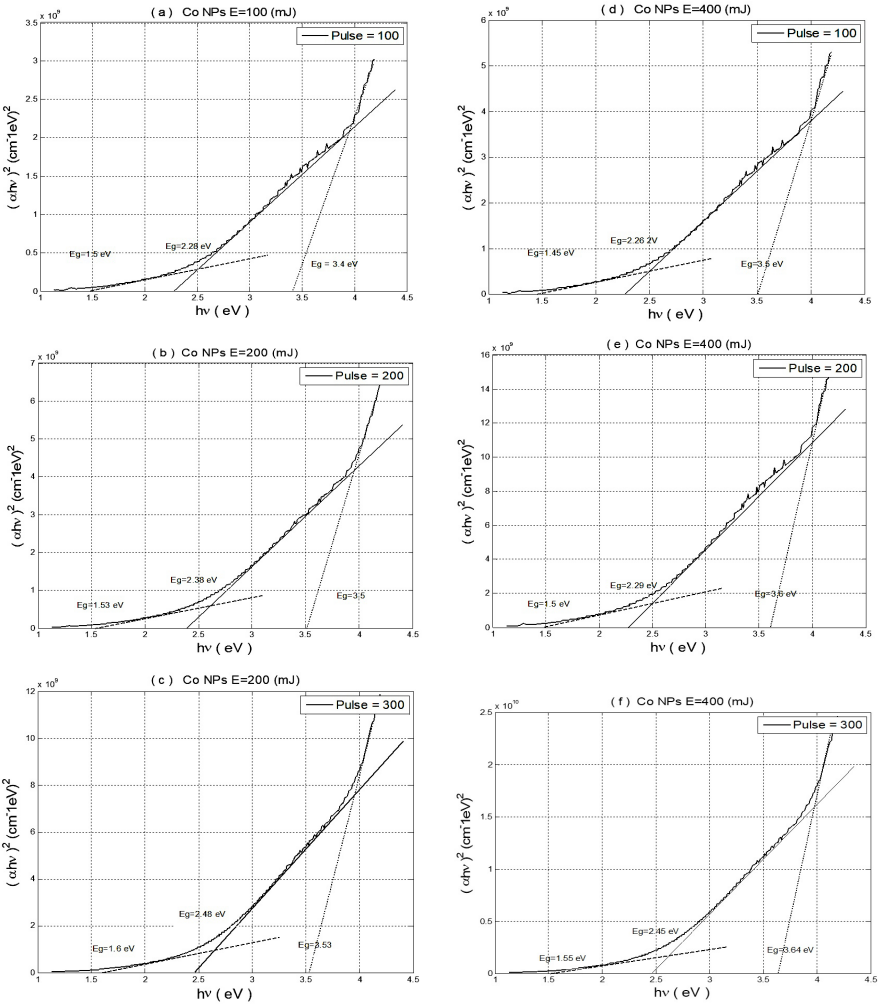

FIGURE 4. *Evaluation of the optical energy gap for (a to c) pulse energy 200 mJ using 100, 200, 300 pulses respectively, (d to f) pulse energy 400 mJ using 100, 200, and 300 pulses respectively*

The refractive index (n) is related to the reflectance (R) and the extinction coefficient (K) through the relation [58].

$$n = \left[\frac{1+R}{1-R}\right] + \left[\frac{4R}{(1-R)^2} - K^2\right]^{1/2} \tag{6}$$

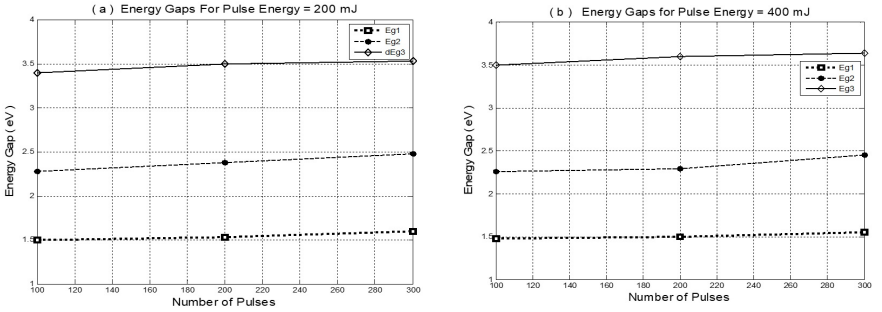

FIGURE 5. *Variation of optical energy gap with pulse energy and the number of pulses (a) for 200 mJ, (b) for 400 mJ*

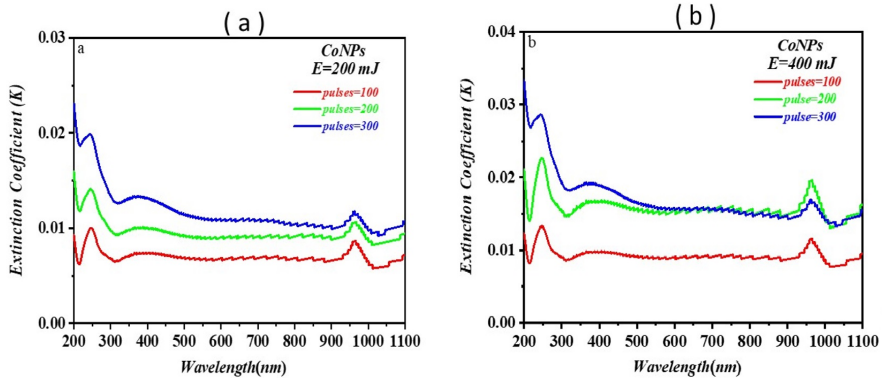

FIGURE 6. *Extinction coefficient (K) for (a) $E = 200$ mJ, (b) $E = 400$ mJ*

The relations of the refractive index to wavelength for the two pulse values and the three pulse numbers are shown in Figure 7.

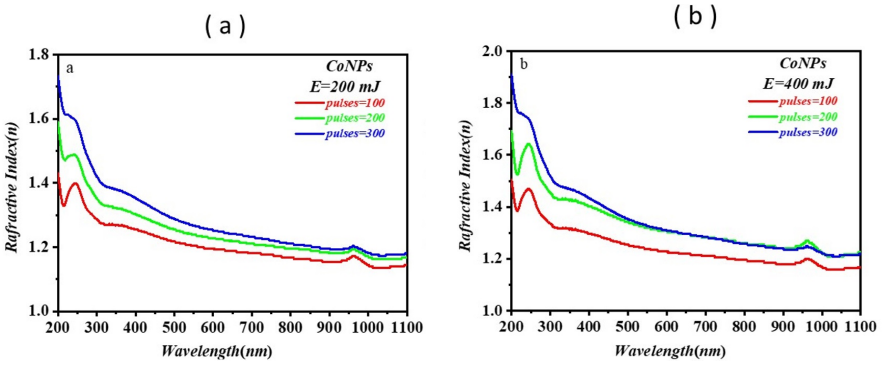

FIGURE 7. *The refractive index (n) for (a) $E = 200$ mJ, (b) $E = 400$ mJ*

Values of the electrical conductivity (σ) given by equation(7) [59] are presented in Figure 8.

$$\sigma = \frac{\alpha n c}{4\pi} \tag{7}$$

With (c) being the speed of light.

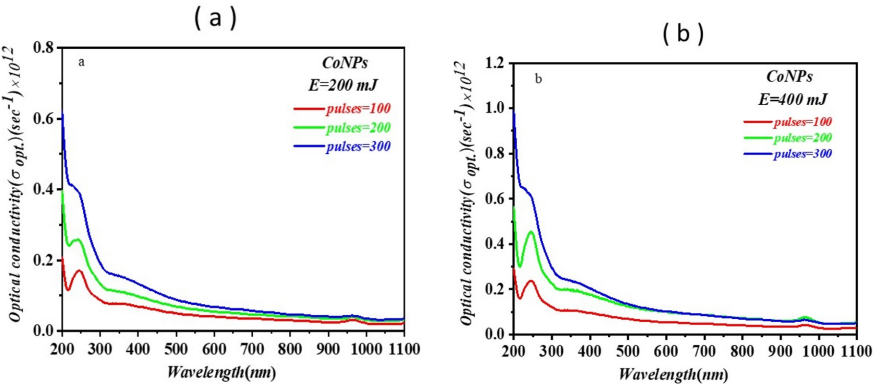

FIGURE 8. *The optical conductivity (σ) for (a) $E = 200$ mJ, (b) $E = 400$ mJ*

The absorbance values obtained are generally consistent with those reported for Co_3O_4, synthesized via the hydrothermal method by Hamdan and Ali [60].

However, the extinction coefficient and refractive index values observed in this study are systematically and significantly lower than those reported at similar wavelengths by Zhu *et al.* [52] and Yamamoto *et al.* [61]. This discrepancy is not unexpected, as optical properties are highly influenced by particle size and particle density within the sample. Although different synthesis methods and experimental conditions can yield similar basic nanostructures, the aggregation, size, and density of particles can vary widely, leading to differences in optical measurements.

Field emission scanning electron microscopy (FE-SEM)

The success of the preparation process of the nanostructure needs to be confirmed before proceeding to carry out any further measurements. This goal is achieved through the use of electron

microscope imaging and X-ray diffraction techniques. Typical field emission electron microscope images for two nanostructure samples prepared using 300 laser pulses with 200 and 400 mJ/pulse are shown in Figure 9. The corresponding grain size analysis for the two samples is shown in Figure 10.

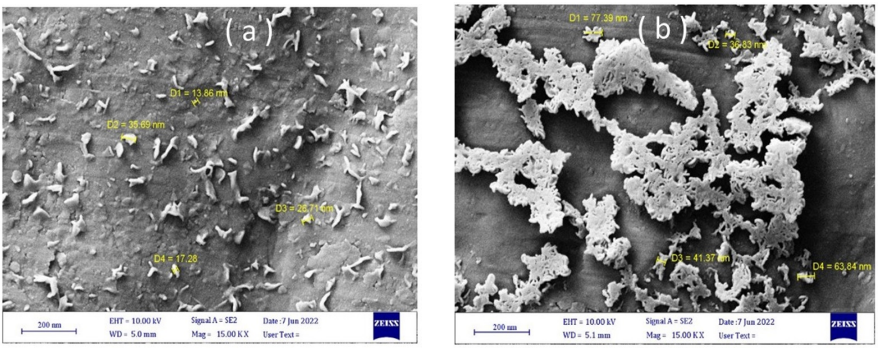

FIGURE 9. *FE-SEM images of CoNPs prepared using 300 laser pulses with pulse energies of (a) 200 mJ, (b) 400 mJ*

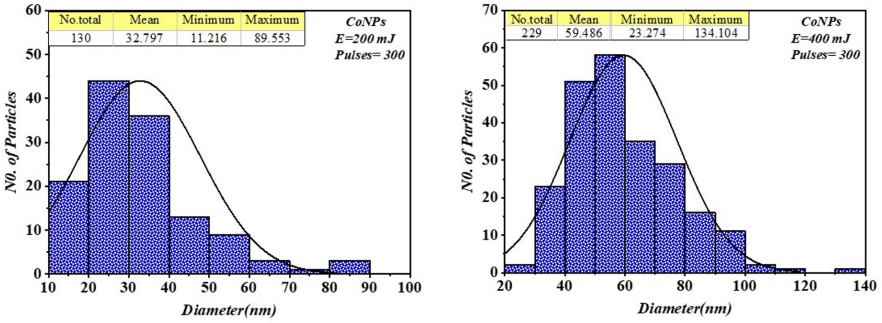

FIGURE 10. *Grain size distributions of CoNPs prepared using 300 laser pulses with pulse energies of (a) 200 mJ, (b) 400 mJ*

X-ray diffraction study

The structural property measurement instruments used was Shimadzu (Japan) XRD-6000, which has the following characteristics: Target: Cu- BF2.7KW, X-ray wavelength: 1.54060 Å, Speed: 5 deg/min, Anode Voltage: 60 kV, Current: 80 mA, Range (2θ): 10°–80°.

Post to the above confirmation of the prepared structures grain size having the acceptable range of nanoparticles, XRD measurements are carried out to establish the successful formation of crystalline Cobalt oxides nanostructures. Typical measurement results for the two samples discussed above are presented in Figure 11.

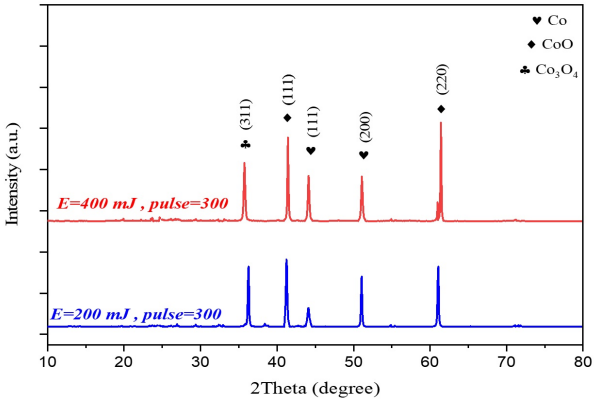

FIGURE 11. *Typical XRD spectrum of samples prepared*

The observed XRD spectra demonstrate that, beside the two (111) and (200) Co peaks, the structures contain two (111) and (220) CoO peaks, and one Co_3O_4 structures. These latter two oxides are known to have semiconductor properties. The formation of both CoO and Co_3O_4 phases is a known outcome in PLAL synthesis, particularly when water is used as the liquid medium. The high-energy laser pulses create a localized plasma that interacts with both the target material and the surrounding water. The presence of dissolved oxygen and the rapid cooling during ablation promote the formation of multiple oxidation states. Therefore, the PLAL method in aqueous media often results in mixed oxide phases due to the dynamic oxidation environment.

The full details of the XRD analysis are given in Table 1 (a and b). The average crystallite size D_{av} of cobalt oxide nanoparticles was calculated from Debye Scherrer's equation (8). XRD measurements confirm the presence of both CoO and Co_3O_4 nanostructures, with average sizes ranging from 30 to 60 nm, in good agreement

with values reported using other preparation methods, such as solution-based chemical reduction [62], thermal deposition [63], and electroplating [64].

$$D_{av} = \frac{k\lambda}{\beta \cos\theta} \tag{8}$$

(a) E = 200 mJ				
Exp. 2Th. (deg.)	FWHM (deg.)	h k l	Ch. name	Crystallite Size (nm)
36.91	0.179	1 1 3	Co_3O_4	46.72
42.34	0.181	1 1 1	CoO	47.06
44.04	0.257	1 1 1	Co	33.30
51.06	0.144	2 0 0	Co	60.96
61.07	0.168	2 2 0	CoO	54.90
Average Crystallite Size (nm)				48.58

(b) E = 400 mJ				
Exp. 2Th. (deg.)	FWHM (deg.)	h k l	Ch. name	Crystallite Size (nm)
36.28	0.221	3 1 1	Co_3O_4	37.74
42.82	0.154	1 1 1	CoO	55.19
44.21	0.153	1 1 1	Co	56.04
51.13	0.117	0 2 6	Co	75.26
61.39	0.122	2 2 0	CoO	76.98
Average Crystallite Size (nm)				60.24

TABLE 1. *(a and b) Detailed XRD analysis parameters for the samples in Figure 11*

Conclusion

The results presented here demonstrate the effectiveness of the PLAL method for preparing cobalt oxide nanostructures. The PLAL method is an effective tool for synthesizing cobalt oxide nanostructures. Experimental parameters, such as laser pulse energy and the number of pulses significantly impact the macroscopic optical properties, including refractive index, absorbance, absorption coefficient, and extinction coefficient of the samples, while having a comparatively smaller effect on the intrinsic properties of the optical energy gaps. Three energy gaps, with mean values of 1.53, 2.36, and 3.53 eV are reported for the cobalt oxide nanostructures in this study. These values align well with corresponding values published in the literature. The results indicate that, although the energy gap values show a slight increase with an increasing number of laser pulses, only minimal differences are observed between the energy gaps produced with laser pulse energies of 200 and 400 mJ/pulse. However, nanostructures synthesized with 400 mJ/pulse exhibit a significantly larger mean grain size radius of about 60 nm, compared to about 33 nm for samples prepared with 200 mJ/pulse, for an equal number of pulses.

Conflict of Interest

The authors declare no conflict of interest.

Acknowledgements

The authors thank the University of Mosul, College of Education for Pure Science, Department of Physics for some supporting this work.

References

[1] A. Haleem, M. Javaid, and et al., Glob. Health J. **7**, 70 (2023).
[2] S. Anjum, S. Ishaque, and et al., Pharmaceuticals **14**, 707 (2021).

[3] K. Lozovoy, Int. J. Mol. Sci. **25**, 9931 (2024).
[4] X. J. Liang, A. Kumar, and et al., J. Nanomater. **2012**, 921897 (2012).
[5] K. McNamara and S. A. M. Tofail, Adv. Phys. **2**, 54 (2017).
[6] F. Eker, H. Duman, E. Akdaşçi, and et al., Molecules **29**, 3482 (2024).
[7] Payal and P. Pandey, Recent Pat. Nanotechnol. **16**, 45 (2021).
[8] A. Aseev, Her. Russ. Acad. Sci. **76**, 318 (2006).
[9] M. Bohr, IEEE transactions on Nanotechnology **1**, 56 (2002).
[10] D. S. Grewal, J. Biosens. Renew. Sources **1**, 114 (2022).
[11] L. Wang, M. P. R. Teles, and et al., Sustain. Energy Technol. Assess. **54**, 102864 (2022).
[12] V. K. Sethi, M. Pandey, and P. Shukla, Int. J. Chem. Eng. Appl. **2**, 77 (2011).
[13] M. A. Al-Jubbori, N. A. Al-Jubbori, and et al., J. Educ. Sci. **34**, 18 (2025).
[14] N. Dewan, J. Kamboj, and J. Kesari, Int. Res. J. Eng. Technol. **8**, 2204 (2021).
[15] U. Banin, N. Waiskopf, and et al., Nanotechnology **32**, 042003 (2020).
[16] M. A. Al-Jubbori and N. A. Al-Jubbori, J. Educ. Sci. **31**, 1 (2022).
[17] B. L. Dinesha, H. Sharanagouda, and et al., Int. J. Curr. Microbiol. Appl. Sci. **6**, 4868 (2017).
[18] I. Gehrke, A. Geiser, and A. Somborn-Schulz, Nanotechnol. Sci. Appl. **8**, 1 (2015).
[19] Nishu and S. Kumar, Hybrid Adv. **3**, 100044 (2023).
[20] I. Tlili and T. A. Alkanhal, J. Water Reuse Desal. **9**, 232 (2019).
[21] A. Bhatnagar, M. Tripathi, and et al., in *Nanotechnol. Electron. Appl.* (Springer, 2022) pp. 29–48.
[22] S.-J. Cho, M.-J. Uddin, and P. Alaboina, in *Emerging Nanotechnologies in Rechargeable Energy Storage Systems* (Elsevier, 2017) pp. 83–129.

[23] M. Al-Jubbori and D. Al-Jubbori, J. Educ. Sci. **31**, 105 (2022).
[24] P. Kumar, H. K. Channi, and et al., Int. J. Low-Carbon Technol. **19**, 747 (2024).
[25] K. Wong and S. Dia, J. Energy Resour. Technol. **139**, 014001 (2017).
[26] V. Gupta, S. Mohapatra, and et al., Gels **8**, 173 (2022).
[27] L. Salvioni, L. Morelli, and et al., Adv. Colloid Interface Sci. **293**, 102437 (2021).
[28] D. E. Effiong, T. O. Uwah, and et al., Adv. Nanoparticles **9**, 1 (2020).
[29] C. Cardoza, V. Nagtode, and et al., Health Sci. Rev. **4**, 100051 (2022).
[30] R. Yadwade, S. Gharpure, and et al., Nano Express **2**, 022003 (2021).
[31] H. A. Yousef, H. M. Fahmy, and et al., Int. J. Trop. Insect Sci. **43**, 1387–1399 (2023).
[32] C. An, C. Sun, and et al., J. Nanobiotechnol. **20**, 11 (2022).
[33] M. Chaud, E. B. Souto, and et al., Toxics **9**, 131 (2021).
[34] K. Harini, K. Girigoswami, and et al., J. Plant Protect. Res. **63**, 137 (2023).
[35] B. Huang, F. Chen, and et al., Nanomaterials **8**, 102 (2018).
[36] M. A. Islam, M. Zuba, and et al., Nanotechnology **29**, 075403 (2018).
[37] H. Chen, W. Wang, and et al., Nanomaterials **12**, 2042 (2022).
[38] S. Amiri, H. Shokrollahi, and et al., Mater. Sci. Eng. C **33**, 1 (2013).
[39] D. Piché and et al., ACS Appl. Mater. Interfaces **11**, 6724 (2019).
[40] Z. Liang, D. Shen, and et al., Nano Res. **17**, 2234 (2024).
[41] X. Peng, X. Jin, and et al., J. Catal. **398**, 54 (2021).
[42] K. Ajaj, M. Al-Jubbori, and et al., J. Laser Appl. **35**, 042055 (2023).
[43] K. Ajaj, A. M. Ali, and et al., Nanosistemi, Nanomateriali, Nanotehnologii **22**, 209 (2024).

[44] K. Ajaj, M. Al-Jubbori, and et al., Radiat. Phys. Chem. **216**, 111384 (2024).

[45] F. A. Mohammed, K. Ajaj, and et al., Russ. Phys. J. **67**, 1015 (2024).

[46] M. A. Al-Jubbori, O. Ayed, and K. Ajaj, Radiat. Phys. Chem. **226**, 111358 (2025).

[47] K. Ajaj, M. Al-Jubbori, and et al., Nanosistemi, Nanomateriali, Nanotehnologii **22**, 557 (2024).

[48] A. H. A. Darwesh, P. A. Mohammed, and et al., Coatings **13**, 578 (2023).

[49] A. Vennela, D. Mangalaraj, and et al., Int J Electrochem Sci. **14**, 3535 (2019).

[50] A. Vennela, D. Mangalaraj, and et.al, Int. J. Electrochem. Sci. **14**, 3535 (2019).

[51] R. Bhargava, S. Khan, and et al., in *AIP Confe. Proc.*, Vol. 1953 (2018) p. 030034.

[52] X. Zhu, J. Wang, and et al., Opt. Mater. Express **2**, 103 (2012).

[53] R. Bhargava, S. Khan, and et al., AIP Conf. Proc. **1953**, 030034 (2018).

[54] M. Yarestani, A. D. Khalaji, and et al., J. Sci., Islam. Repub. Iran **25**, 339 (2014).

[55] D. Letsholathebe, F. Thema, and et al., Mater. Today: Proc. **36**, 499 (2021).

[56] G. Hitkari, S. Sandhya, and et al., J. Mater. Sci. Eng. **7**, 419 (2018).

[57] L. Qiao, H. Y. Xiao, and et al., J. Mater. Chem. C **1**, 4628 (2013).

[58] I. Saini, J. Rozra, and et al., Mater. Chem. Phys. **139**, 802 (2013).

[59] M. Rashidian and D. Dorranian, J. Theor. Appl. Phys. **8**, 121 (2014).

[60] S. A. Hamdan and I. M. Ali, Iraqi J. Phys. **17**, 77 (2019).

[61] H. Yamamoto, S. Tanaka, and et al., J. Ceram. Soc. Jpn., Suppl. **112**, S876 (2004).

[62] F. K. Sabir, E. T. Bekele, and et al., J. Nanostruc **11**, 577 (2021).

[63] S. Farhadi, J. Safabakhsh, and et al., J. Nanostruct. Chem. **3**, 69 (2013).

[64] E. Delnavaz and K. Asadpour-Zeynali, Results Chem. **7**, 101321 (2024).